Supplementary material

Supplementary Experimental Procedure

Protein tomography analyses of MHCI, PIR-B, and the PIR-B–MHCI complex- The procedure used for protein tomography analysis improved by Sidec Technologies (Kista, Sweden) was described elsewhere (1). Briefly, either the recombinant 68 kDa PIR-B D1–D6 monomer, biotinylated recombinant H-2L^d/β_2m with peptide TPHPARIGL or H-2D^b/β_2m with peptide ASNENDAM (Proimmune, Oxford, UK), or a 1:1 (w/w) mixture of them incubated overnight at 4°C under rotation was prepared and mixed with colloidal gold particles to facilitate alignment of the micrographs at a protein concentration of 0.35 mg/ml. In some analyses of MHC-I molecules, the biotinylated H-2 complex was also labeled with Streptavidin-Nanogold (Nanoprobes, Yaphank, NY). The solution was applied as a thin film on a sample grid, which was flash frozen in liquid ethane. A tilt-series of electron micrographs was recorded with a Philips CEM200 FEG transmission electron microscope run at extraction and acceleration voltages of 4.48 and 200 kV, respectively. A beam of electrons was passed through the sample and transformed by lenses into an image that was projected onto a detector array. We performed low-dose electron microscopy so that the accumulated dose did not exceed 20–30 e/Å^2 to preserve the atomic structures of proteins throughout the data collection. Samples were rotated through ± 60° and micrographs were captured with a cooled slow-scan camera (2048 × 2048 CCD chip, pixel size 14 μm; TVIPS GmbH, Gauting, Germany) using the EMMENU software at a magnification of 24,900 at 2°-tilt intervals in the range ± 62°, giving a final pixel size of 5.63 Å. Then the micrographs were aligned to construct preliminary 3D tomograms of the proteins using conventional filtered backprojection techniques. Tomograms were then subjected to refinement using the Constrained Maximum Entropy Tomography (COMET) method (2) to improve the signal-to-noise-ratio and reconstruct 3D tomograms. Selected molecules or molecular complexes were rotated through 360° and their 3D conformations were analyzed in more detail.

Supplementary Results

Amino acid sequence of MHCI-binding D1D2 of LILRB is more homologous to PIR-B D1D2 and D3D4 than D5D6. In terms of MHCI binding, PIR-B is considered to be the sole ortholog of the human inhibitory leukocyte Ig-like receptors, LILRB1 and LILRB2 (or ILT2/LIR1 and ILT4/LIR2, respectively), possessing four Ig-like extracellular domains (3–7). Crystallographic analyses have revealed that LILRB1 and LILRB2 bind to human MHCI at their N-terminal two Ig-like domains, D1D2, but not their C-terminal ectodomains, D3D4 (fig. S1A) (3,8–11). On the other hand, both LILRB2 and PIR-B bind to Nogo (12), albeit that it has not been examined whether or not LILRB1 can do this as well. Based on preceding reports by others (13,14) and our analysis (fig. S1B) indicating that the amino acid sequences of MHCI-binding D1D2 of LILRB1 and LILRB2 are equally homologous to PIR-B D1D2 (44.9 and 45.2%, respectively) and D3D4 (43.4 and 46.2%, respectively), but less similar to D5D6 (30.0 and 31.1%, respectively), we hypothesized that both D1D2 and D3D4 of PIR-B could bind to MHCI. However, we found that only D1D2 can bind MHCI (see Fig. 1).

Visualization of the structure of PIR-B–H-2 complex by protein tomography. We attempted to visualize the structure of the PIR-B–H-2 complex by protein tomography analysis (1,15) in order to gain an insight into the overall structure for PIR-B D1D2–H-2 binding. Before analyzing the 3D structure of the PIR-B–H-2 complex, we firstly performed protein tomography analysis of biotinylated H-2D^b, free as well as in a complex with Streptavidin-Nanogold, to determine the conformational orientation, and an x-ray structure was fitted into the selected protein tomograms. The overall conformations of biotinylated MHCI in solution were found to be similar to that of the x-ray structure of crystallized MHCI (16–18) (fig. S2A, B). This conclusion was based on analysis of 278 objects identified as either free MHCI or the complex. Then, we constructed 3D images of the free PIR-B ectodomain in solution by analyzing some objects observed in a PIR-B and MHCI mixture. We compared seven objects with similar structures, two of which are shown in fig. S2C and

D. These structures were long, flexible objects, where the separate six Ig-like domains were resolved as regions with increased density inside the molecule, thus enabling us to identify these objects as PIR-B ectodomains. Based on these data, the overall conformation of the PIR-B ectodomain itself is suggested to be flexible in aqueous solution, and it can be in a stretched out form (fig. S2C) as well as in a shrunk form (fig. S2D). Finally, we utilized these 3D views of the PIR-B ectodomain and an MHCI for structural analysis of PIR-B–MHCI in solution. We examined a total of 27 discrete objects and assigned two of them as PIR-B ectodomains, as described above, one as an MHCI molecule, ten as PIR-B–MHCI complexes, and the rest of them as ambiguous molecule(s). Among the assumed ten PIR-B–MHCI complexes, we could unequivocally identify eight of them as the PIR-B–MHCI complex. A typical example is shown in fig. S2E, where an MHCI is bound to one end of the six Ig-like domains of PIR-B. All of these eight objects had some general features in common: a long tail with Ig-like domains that were often well resolved and a larger volume at one end, which corresponds to an MHCI. This structural data is consistent with the present binding study showing that the N-terminal D1D2 of PIR-B is responsible for MHCI binding.

Supplementary References

1. Sandin, S., Öfverstedt, L. -G., Wikström, A. -C., Wrange, Ö., and Skoglund, U. (2004) *Structure* **12**(3), 409–415
2. Skoglund, U., Ofverstedt, L. G., Burnett, R. M., and Bricogne, G. (1996) *J Struct Biol* **117**(3), 173–188
3. Colonna, M., Nakajima, H., and Cella, M. (1999) *J Leukoc Biol* **66**(5), 718–722
4. Borges, L. and Cosman, D. (2000) *Cytokine Growth Factor Rev* **11**(3), 209–217
5. Wende, H., Colonna, M., Ziegler, A., and Volz, A. (1999) *Mamm Genome* **10**(2), 154–160
6. Long, E. O. (1999) *Annu Rev Immunol* **17**, 875–904
7. Takai, T. (2005) *Immunology* **115**(4), 433–440
8. Colonna, M., and Samaridis J. (1995) *Science* **268**(5209), 405–408
9. Willcox, B. E., Thomas, L. M., and Bjorkman, P. J. (2003) *Nat Immunol* **4**(9), 913–919
10. Shiroishi, M., Tsumoto, K., Amano, K., Shirakihara, Y., Colonna, M., Braud, V. M., Allan, D. S., et al. (2003) *Proc Natl Acad Sci U S A* **100**(15), 8856–8861
11. Willcox, B. E., Thomas, L. M., Chapman, T. L., Heikema, A. P., West, A. P. Jr., and Bjorkman, P. J. (2002) *BMC Struct Biol* **2**, 6
12. Atwal, J. K., Pinkston-Gosse, J., Syken, J., Stawicki, S., Wu, Y., Shatz, C., and Tessier-Lavigne, M. (2008) *Science* **322**(5903), 967–970
13. Dennis, G. Jr., Stephan, R. P., Kubagawa, H., and Cooper, M. D. (1999) *J Immunol* **163**(12), 6371–6377
14. Nikolaidis, N., Klein, J., and Nei, M. (2005) *Immunogenetics* **57**(1-2), 151–157
15. Wartiovaara, J., Ofverstedt, L. G., Khoshnoodi, J., Zhang, J., Makela, E., Sandin, S., Ruotsalainen, V., et al. (2004) *J Clin Invest* **114**(10), 1475–1483
16. Zhang, W., Young, A. C., Imarai, M., Nathenson, S. G., and Sacchettini, J. C. (1992) *Proc Natl Acad Sci U S A* **89**(17), 8403–8407
17. Fremont, D. H., Stura, E. A., Matsumura, M. M., Peterson, P. A., and Wilson, I. A. (1995) *Proc Natl Acad Sci U S A* **92**(7), 2479–2483
18. Young, A. C., Zhang, W., Sacchettini, J. C., and Nathenson, S. G. (1994) *Cell* **76**(1), 39–50

Supplementary Figures

Figure S1

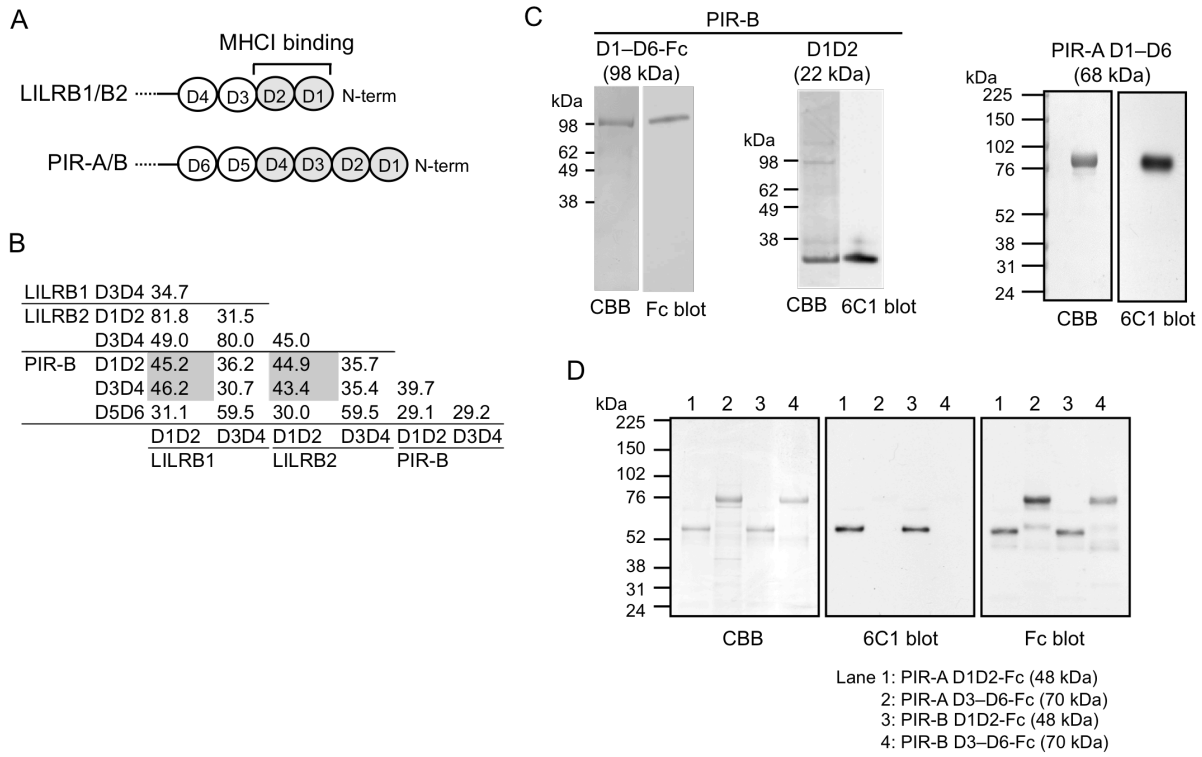

Fig. S1. Schematic views of the ectodomain structures, amino acid homologies among MHCI receptors, and affinity-purified recombinant proteins of PIR-B and PIR-A. (A) Schematic illustration of the domain structures of LILRB1/B2 and PIR-A/B. In the PIR-A/B diagram, gray shading indicates the domains homologous to LILRB1/B2 D1D2, which binds to MHCI–β_2m complexes. (B) Homologies among the amino acid sequences of LILRB1/B2 and PIR-B. The sequences of twin domain units are compared for LILRB1 (GenBank AF009220), LILRB2 (AF000574), and PIR-B from C57BL/6 mice (U83172). D1D2 and D3D4 of PIR-B are relatively homologous (gray squares) to MHCI-binding D1D2 of LILRB1/B2 compared to D5D6. PIR-B D5D6 was more homologous to LILRB1/B2 D3D4, whose function has not been determined yet. (C, D) Affinity-purified recombinant domains of PIR-B and PIR-A. Profiles on Coomassie brilliant blue staining (CBB) or immunoblotting with 6C1 or anti-Fc antibodies are shown.

Figure S2

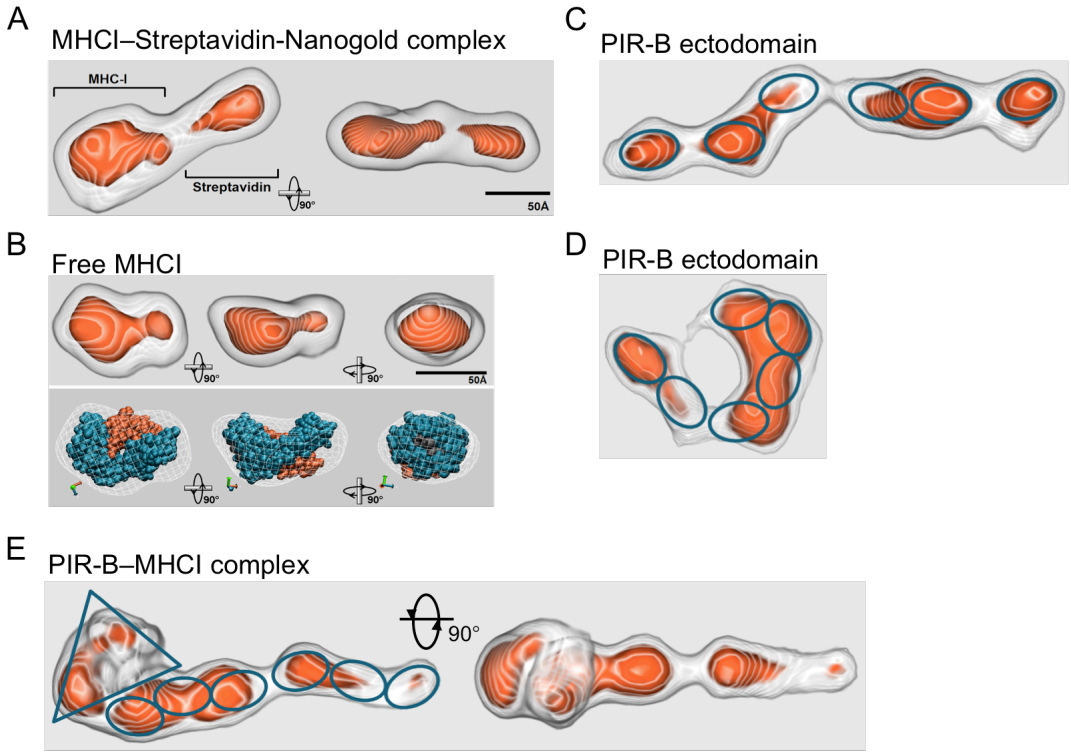

Fig. S2. Flexible nature of PIR-B ectodomain in aqueous solution revealed on protein tomography analysis. (A) Tomograms of an MHCI bound to Streptavidin-Nanogold in two different orientations. The grey semi-transparent contours represent the approximate surface of the protein, and the red volumes are the regions of higher density representing internal protein structures. In the higher density images, the MHCI is observed as a large volume with a smaller bud assigned as the Streptavidin-Nanogold entity. Since the biotinylated C-terminal located on the α3 domain binds to the streptavidin, the α3 domain can be assigned to the region of the bud in the tomograms. (B), Tomogram of a free MHC-I together with the crystal structure of a MHCI, which has been optimally fitted to the tomogram. The crystal structure is shown using a space fill model, in which the α chain is shown in blue and the β_2m chain in red. The overall shape of a free MHCI molecule in solution is similar to that of the crystal structure. (C, D) Tomograms of two typical PIR-B objects found for a PIR-B–MHCI mixture. The approximate positions of the six Ig-like domains are indicated by blue ellipses. In (C), the PIR-B ectodomain appears in a stretched out conformation with a length of about 23 nm. The two flanking Ig-like domains (D1 and D6) are well resolved and appear as small spheres, while the other four Ig-like domains are merged into two separate, D2D3 and D4D5, densities. In (D), the PIR-B ectodomain appears in a bent conformation. The right hand red volume probably contains four Ig-like domains, while the left hand one contains two domains. (E) Tomograms of a typical PIR-B–MHCI complex in solution. The possible MHCI part of the left object is indicated by a blue triangle. The PIR-B ectodomain appears as a long flexible tail where some of the Ig-like domains are resolved as separate objects tentatively indicated by blue ellipses, albeit those possibly in contact with the MHCI mass are hard to ascertain. The exact orientation of the MHCI in the complex cannot be determined with certainty at this level of resolution.

Figure S3

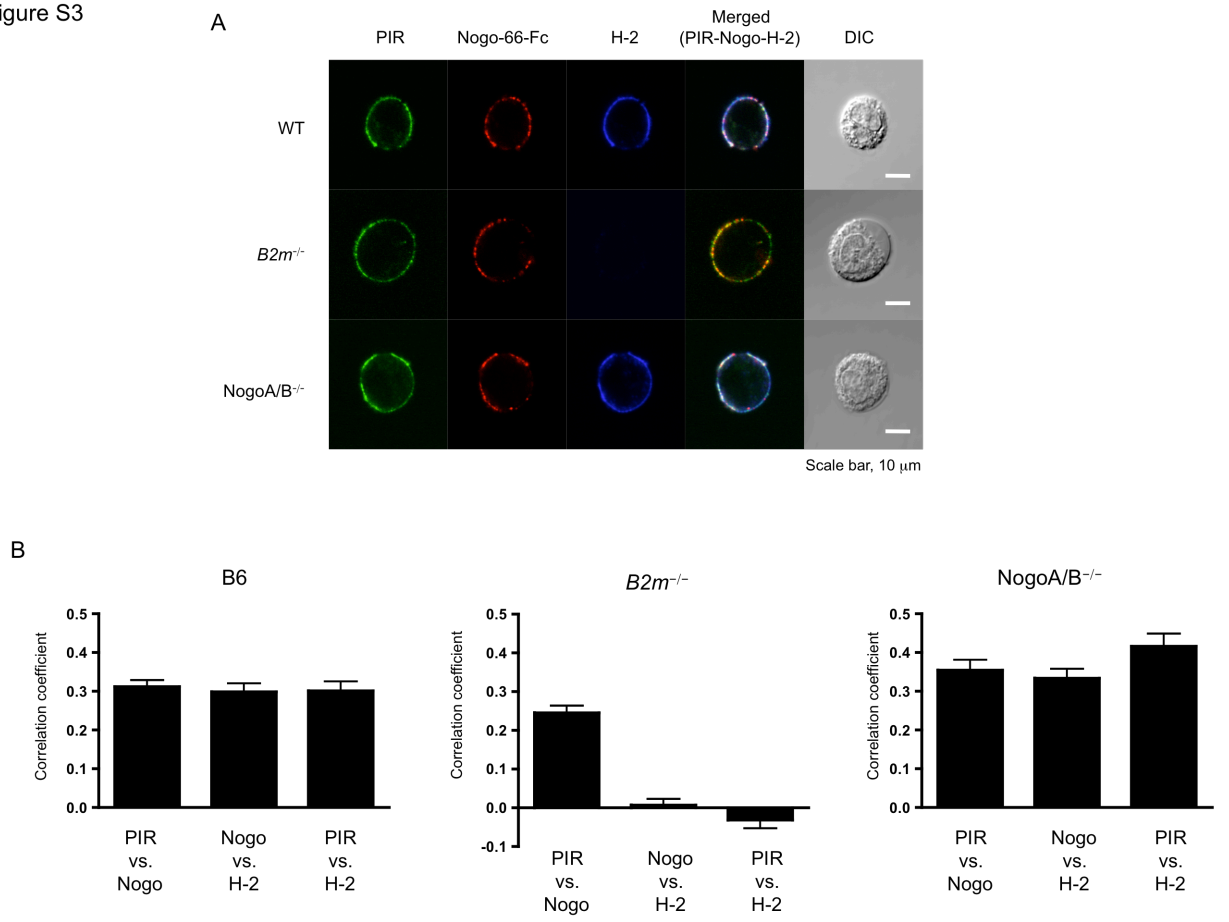

Fig. S3. Confocal imaging of BMMCs showing a partial ternary association of PIR-B, MHCI, and Nogo-66. (A) Confocal imaging of BMMCs. B6, B2m$^{-/-}$, or NogoA/B-deficient (NogoA/B$^{-/-}$) BMMCs were stained with Alexa Fluor 488–conjugated anti–PIR-A/B (6C1), Alexa Fluor 546–conjugated Nogo-66-Fc and Alexa 647–conjugated anti–H-2K^{b}/D^{b} (28-6-8). DIC, differential interference contrast. Scale bar, 10 μm. (B) Correlation coefficients calculated for the colocalization of PIR-A/B, Nogo66-Fc protein, and H-2K^{b}/D^{b} are shown (n = 15). Data are shown as mean ± SEM. PIR-B was clearly co-localized within a pixel (about 20 nm) with MHCI on the same cell surface of BMMCs (A) with a nice correlation between two signals (B) as described previously (24). PIR-B was also co-localized with Nogo-66 (A) with a clear correlation of the signals (B). Importantly, a part of the PIR-B signal was also co-localized with MHCI and Nogo-66 signals (A, light blue patches, and B), suggesting that a fraction of PIR-B binds simultaneously to MHCI and Nogo-66.

Figure S4

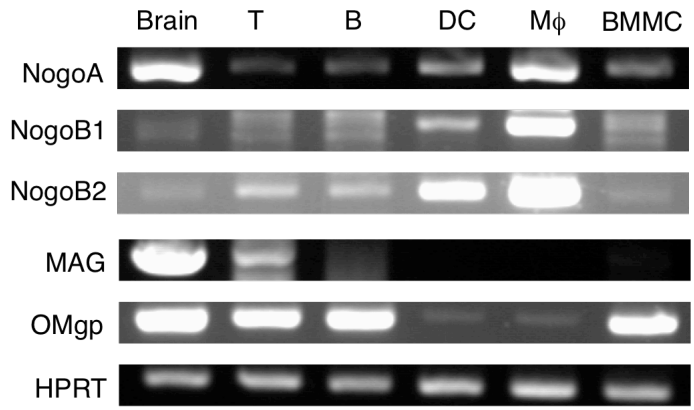

Fig. S4. mRNAs for Nogo isoforms, MAG, and OMgp were detected in cells of the immune system. Expression of mRNAs for Nogo isoforms (NogoA, B1, and NogoB2), MAG, and OMgp in cells of the immune system was examined. Splenic $CD19^+$ B cells, Thy-1^+ T cells, bone marrow-derived dendritic cells (DC), bone marrow-derived macrophages (Mϕ), and BMMCs from B6 mice were subjected to RT–PCR. Brain extracts were used as positive controls for mRNAs for NogoA, MAG, and OMgp. The mRNA for hypoxanthine-guanine phosphoribosyltransferase (HPRT) was monitored for standardization.